
Functional Connectome: Approximating Brain Networks with Artificial Neural Networks

Sihao Liu (Daniel)

Research Department of Cell and Developmental Biology
University College London
sihao.liu.18@ucl.ac.uk

Augustine N. Mavor-Parker

Research Department of Cell and Developmental Biology
Centre for Artificial Intelligence
University College London

Caswell Barry

Research Department of Cell and Developmental Biology
University College London

Abstract

We aimed to explore the capability of deep learning to approximate the function instantiated by biological neural circuits - the functional connectome. Using deep neural networks, we performed supervised learning with firing rate observations drawn from synthetically constructed neural circuits, as well as from an empirically supported Boundary Vector Cell–Place Cell network. The performance of trained networks was quantified using a range of criteria and tasks. Our results show that deep neural networks were able to capture the computations performed by synthetic biological networks with high accuracy, and were highly data efficient and robust to biological plasticity. We show that trained deep neural networks are able to perform zero-shot generalisation in novel environments, and allows for a wealth of tasks such as decoding the animal’s location in space with high accuracy. Our study reveals a novel and promising direction in systems neuroscience, and can be expanded upon with a multitude of downstream applications, for example, goal-directed reinforcement learning.

1 Introduction

Artificial deep neural networks (DNNs) [1] have been successfully applied to a range of domains including image recognition [2], speech and language processing [3] and reinforcement learning [4]. Despite these success stories, the systems neuroscience community has been skeptical about deep learning being the solution to understanding intelligence in the brain. This is because of the simplification of individual neurons in these models as well as the biological plausibility of the back-propagation training algorithm [5]. Nevertheless, DNNs (ReLU networks) are powerful tools as approximators [6] despite abstracting away details from biology.

We explore how the architectures, including widths and depths of an arbitrary neuronal circuit corresponds to a DNN. We begin by constructing a rate network with additional features corresponding to sensory processing in the brain—which we call an *Approximate Biological Neural Network*

(ABNN)—and generate synthetic input and output patterns using simulated spike trains. We fit two classes of DNNs, Multi-Layer Perceptrons [7] (MLPs) and Long Short-Term Memory [8] networks (LSTMs) with various numbers of depths and widths are fitted to learn these patterns. We examine the data efficiency the approximating DNNs and how they generalise when the ABNN undergoes small plasticity changes. After, we simulate an experimentally supported rate network in the mammalian hippocampal formation—the Boundary Vector Cell model [9]—and fit the DNNs to the firing rates of the downstream place cells. Further, we demonstrate that the learned DNNs are able to perform a range of tasks related to the hippocampal formation, such as decoding the trajectory of an agent in an environment.

A DNN substituted neuronal circuit is useful as it allows fast and non-invasive experimental neuroscience research. We hope this preliminary work give rise to further research in complicated, hierarchical models of biological neural circuits, as well as applying the approaches developed to *in vivo* experimental data rather than just theoretical models of neural circuits.

1.1 Related Works

Existing works focuses on modelling single the behaviour of single neurons—Beniaguev et al. [10] demonstrated that a 3D-reconstructed rate layer 5 cortical pyramidal neuron with NMDA receptors can be best captured by a ReLU network with 7 hidden layers and 128 hidden units each. Removing NMDA receptors allows the neuron to be learned by a much smaller deep network with a single hidden layer and 128 units. Moldwin et al. [11] implemented the perceptron learning algorithm [7] on a biophysical model of a simulated layer 5 pyramidal cell using the NEURON [12] software package and found that the biophysical perceptron was able to achieved results comparable to a traditional perceptron model. Wang et al. [13] successfully predicted the spike features as well as the dropping intervals in 9 simulated Hodgkin-Huxley neurons with different ion channel settings using a DNN trained on spike voltage data, which they dubbed Feature Prediction Module.

2 Methods

Our experiments as structured as follows. First, we construct a series of deep learning models, that we call Approximate Biological Neural Networks (ABNNs), which contain features that make them somewhat more biologically plausible. Then we systematically study the ability of a separate neural network to learn to perform the same mapping as the ABNNs. After, we repeat this procedure for a more biologically plausible model of circuits in the hippocampal formation.

2.1 Learning an Approximate Biological Neural Network

The base structure of our ABNN resembles a MLP with 16 input neurons, 16 output neurons, and 4 layers of 256 hidden units each. On top of this scaffold we consider augmenting the following network properties.

1. Variations between neurons. Neurons tend to have different biophysical properties, such as axonal length and membrane conductivity [14], that result in different firing behaviours. We model these biophysical difference by assigning each neuron in each layer a distinct transfer function [15]. These are sampled randomly from ReLU, ELU, SiLU, CELU, Sigmoidal, Tanh and Leaky ReLU with leak parameters 0.1, 0.2 and 0.3.
2. Excitatory and inhibitory synapses. We consider the fact that various types of neurotransmitters govern whether the activation of a pre-synaptic neuron invoke excitatory or inhibitory responses in the post-synaptic neuron [16]. The weights between neuron i in the previous layer and neuron j in the next layer is initialised using a unit Gaussian: $w_{ij} \sim \mathcal{N}(0, 1) \forall i, j$.
3. Feed-forward connections that resemble the hierarchical architectures of mammalian neocortex [17] [18]. For example, an ABNN with feedforward connections has 16 input neurons, projecting sequentially to 4 hidden layers of 256 neurons each, and to an output layer of 16 layers.
4. Skip connections [19]. Additional weights are initialised to downstream layers using the same schemes as above

5. Feed-back connections [17]. We allow the neurons in downstream layers to project back to upstream layers, with the same weight initialisation scheme. This correspond to the observation of large number of recurrent connections in the brain.
6. Sparsity. Real neurons in the brain are sparsely connected [20]. Each connection is randomly dropped with probability 0.5. This feature is added based on the fact that neuronal connections in the brain are highly sparse.
7. Lateral inhibitions [17]. We additionally allow each neuron i in a hidden layer to connect to every other neuron in the same layer, with negative weight:

$$w_{ij} \sim \mathcal{N}\left(-1 + \frac{|i-j|}{N}, 1\right) \quad \forall i, j \quad i \neq j \quad (1)$$

Where N is the total number of neurons in that layer. That is, any central neuron inhibits its neighbours. This feature follows from the observation that lateral inhibition is ubiquitous in early sensory areas.

Figure 1 shows an illustration of an ABNN architecture with the different design choices described above being color coded.

Synthetic Biological Data To mimic the information processing in a biological neural network, we use the number of spikes from each neuron as the input pattern to our ABNN described below. We assume the number of spikes encode the value of the external stimulus (*rate coding*). To produce variable spike input patterns, spike trains are simulated from a point process with Gamma-distributed inter-spike intervals [21], which mimics the refractory period of real neuron firings [22]. Specifically, the inter-spike intervals t_i for each neuron i in the input layer to follow a Gamma distribution:

$$t_i \sim \Gamma(\alpha_i, \beta_i) \quad \forall i \quad (2)$$

Where the mean firing rate for each input neuron i has a mean firing rate r_i , sampled from a Gaussian:

$$\mathbf{E}(t_i) = \frac{\alpha_i}{\beta_i} = r_i \sim \mathcal{N}(10, 1) \quad \forall i \quad (3)$$

The simulated spike timings for each neuron are then time-binned to produce input patterns. Thus, each input pattern consists of vectors of spike counts produced by 16 neurons in 50 time steps. These patterns are fed into the ABNN to producing “raw” output patterns from each of the 16 output neurons. A small Gaussian noise ($\sigma = 0.01$) is added to the raw output patterns to model neural noise in the information passing process [23], which are then normalised (Z-scored) to use as training labels.

An Assortment of Approximate Biological Neural Networks We construct 4 ABNNs, each with increasing complexity, following the properties described. These are summarised in Table 1 For each ABNN, we use the same input neuron patterns, and generated 10,000 pairs of input-output patterns as training set, 1,000 as the validation set and 1,000 as test set.

Table 1: Summary of structures or properties included with each ABNN.

	Var.	Ex. & in.	FF	Spar.	Skip	FB	LI	Noise
Feed-forward ABNN	✓	✓	✓	✓				✓
Skip ABNN	✓	✓	✓	✓	✓			✓
Feed-back ABNN	✓	✓	✓	✓		✓		✓
Complex ABNN	✓	✓	✓	✓	✓	✓	✓	✓

Training Procedure To explore how we can exploit the power of deep learning, we trained various multi-layer perceptrons with varying width (number of hidden units) and depth (number of hidden layers). For the feed-back and complex ABNN, we also trained recurrent neural networks with an additional LSTM layer followed by varying numbers of linear layers. This follows from the inclusion of recurrent architectures in the ABNNs, which induces temporal dependency between trials. The LSTM layer has the same number of hidden units as the rest of the network. All deep neural networks have ReLU non-linearities and are trained with a mean squared error loss function. For all ABNN experiments, we use the Adam optimiser [24] with learning rate 0.001 and batch size 200, unless stated otherwise. Parameter search was run with a range of hidden layers [1, 2, 3, 4, 5, 6, 7, 8] and

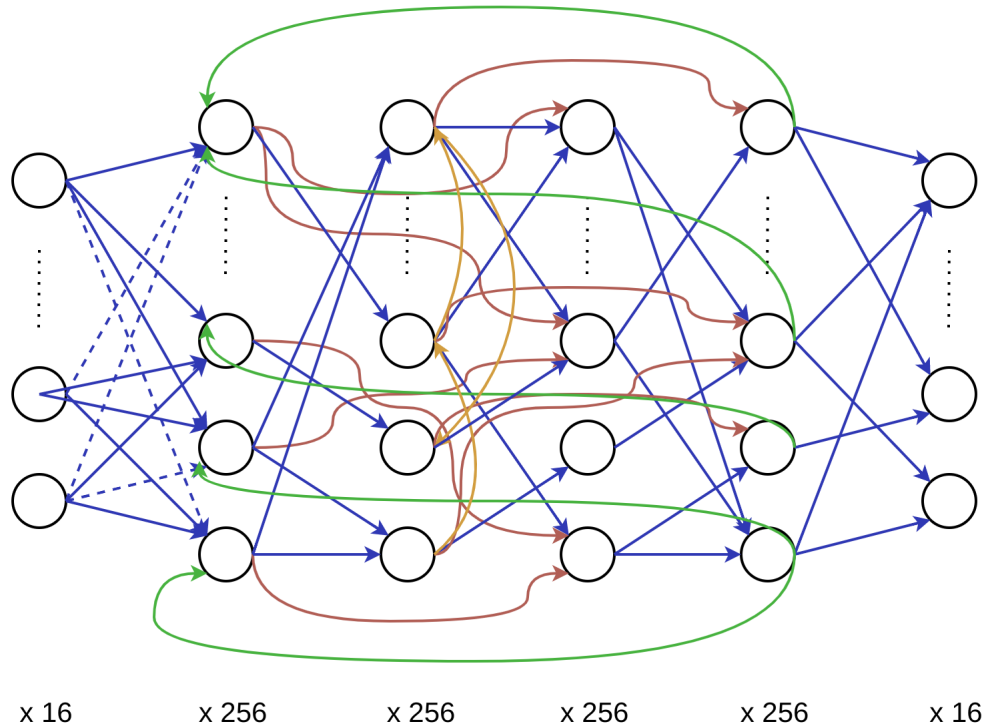


Figure 1: The structure of a full complex arbitrary neural circuit. Left is a simplified diagram showing information flow and right represents detailed connections between each layer, where (A) blue lines represent feed-forward connections; (B) dotted lines indicate weights dropped to zero to comply with sparsity and is not shown for subsequent layers to avoid cluttering; (C) red curves indicates skip connections between layers 1 and 3 as well as 2 and 4; (D) amber curves indicate lateral inhibition in layer 2; (E) green curves indicate feed-back connections from layer 4 to layer 1. The number of neurons in each layer is shown in the middle and not to scale in the right diagram.

hidden units [2, 4, 8, 16, 32, 64, 128, 256]. The best combination of hyper-parameters is chosen by picking the set of parameters that minimised the mean final MSE loss on the test set. These networks are then trained on the training set, and the mean final MSE losses on the test set are reported. These are produced by averaging the MSE loss after training for 50 epochs over 30 repeats to ensure reliability.

Data Efficiency, Generalisation and Plasticity We performed additional experiments on the complex ABNN and the corresponding trained DNNs. First, we explore the data efficiency of learning networks: DNNs are trained for up 1,000 epochs using a subset n of the 10,000 training data vectors generated by the complex ABNN, drawn randomly without replacement and their performance were via MSE loss when predicting on the full, 1,000 data vectors test set. The number of data vectors drawn are $n = 1, 5, 10, 50, 100, 200, 400, 800, 1600, 3200, 6400$. Secondly, we explore how the trained DNNs perform when plasticity changes occur in the complex ABNN. We model change by injecting a Gaussian random variable to each established connections:

$$w_{ij} = w_{ij} + \delta w_{ij}, \quad \delta w_{ij} \sim \mathcal{N}(0, \sigma^2) \quad \forall i, j : w_{ij} \neq 0 \quad (4)$$

Where neuron i and j are connected. Another view of the weight change experiment is how well the DNNs can cope with random noises in the ABNN. The original input patterns are then passed through the altered ABNN and normalised again. The architecture and transfer function of the neurons are kept unchanged. σ is systematically discretised in a logarithmic scale from $e^{-7.0}$ to $e^{4.0}$ and the performance of the trained DNNs are compared with randomly initialised ones. The experiment is repeated 30 times and the mean and standard deviation are taken to improve reliability.

2.2 Learning the Boundary Vector Cell model

Next, we turn to an empirically supported model of the cortical circuit, the Boundary Vector Cell model[9]. Boundary vector cells are crucial for an animal’s ability to self-localise in an environment. Analogous to the ABNN experiments, we run parameter search and train DNNs on the input-output pairs of the neural circuit in a supervised manner, using randomly sampled locations in an environment. We measure the generalisability of our approximations by making predictions in novel unseen environments and comparing the predictions to the ground truth from the BVC model.

Simulated Boundary Vector Cells and Place Cells Boundary vector cells [25] are a type of pyramidal neurons found in the subiculum and entorhinal cortex of mammalian hippocampal formation. They respond to the presence of boundaries in an environment at a preferred distance d_i and preferred bearing ϕ_i (in radians). The firing contribution g_i of a small segment of the boundary subtending a small angle $\delta\theta$, with distance r and bearing θ can be described with a tuning function.

$$g_i(r, \theta) \propto \frac{\exp[-(r - d_i)^2 / (2\sigma_{\text{rad}}^2(d_i))]}{\sqrt{2\pi\sigma_{\text{rad}}^2(d_i)}} \times \frac{\exp[-(\theta - \phi_i)^2 / 2\sigma_{\text{ang}}^2]}{\sqrt{2\pi\sigma_{\text{ang}}^2}} \quad (5)$$

The overall firing rate of a boundary vector cell f_i at a location \mathbf{x} is obtained by integrating over all over all angles:

$$f_i(\mathbf{x}) = \int_0^{2\pi} g_i(r, \theta) \delta\theta \quad (6)$$

Boundary vector cells project to place cells [26], another type of pyramidal neuron in the hippocampus proper. In [25]’s model, the firing rate of a place cell F_j is a thresholded sum of the firing rate of upstream boundary vector cells:

$$F_j(\mathbf{x}) = \left[A \sum_{i=1}^N w_{ij} f_i(\mathbf{x}) - T_j \right]_+ \quad (7)$$

Where T_j is the threshold and $[\cdot]_+$ denotes the non-linear rectifier. We simulate 100 boundary vector cells and 10 place cells. Each boundary vector cell i has preferred distance d_i and angle ϕ_i sampled from continuous uniform distribution:

$$d_i \sim \mathcal{U}(0, 3200) \quad \phi_i \sim \mathcal{U}(0, 2\pi) \quad \forall i = 1, \dots, 100 \quad (8)$$

Each place cell j is randomly connected to $N = 15$ BVCs. The connection weights are sampled according to a normal distribution:

$$w_{ij} \sim \mathcal{N}(1, 1) \quad (9)$$

The multiplier is chosen to be $A = 10,000$ and the threshold T_j is capped at 80% of the firing capacity of that place cell [27]. The rate map of the resulting place cells are illustrated in Figure 2.

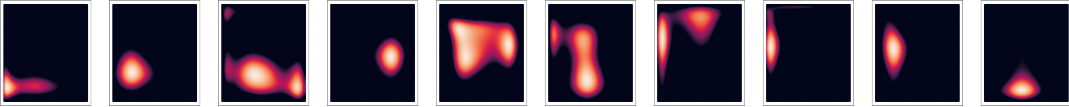


Figure 2: Bird’s eye view of the firing fields of 10 Place Cells in a simulated square environment.

We sample random locations in a $3,200 \times 3,200$ mm square environment, and simulate the firing rates of the boundary vector cells and place cells as input and output patterns, respectively. 10,000 pairs are sampled as the training set, 1,000 pairs for the validation set and 1,000 pairs for the test set.

Training Deep Networks We perform hyper-parameter search on a range of multi-layer perceptrons with hidden linear layers [1, 2, 3, 4, 5, 6, 7, 8] with a range of hidden units [1, 2, 4, 8, 16, 32, 64, 128, 256], mapping from an 100 input neuron firing rates to 10 output neuron firing rates. We trained these networks on the validation set for 100 epochs and find the network with the best combination of hyperparameters over 30 repeats. This network is then trained with the training set data and tested using various tasks. In all training, mean squared error is used as the loss function and Adam [24] with learning rate 0.001 is used as the optimiser.

Generalisation in Unseen Environments We test the generalisation performance of the trained DNN in unseen environments. The 10 place fields are predicted on two groups of environments. In the first group, we stretch and compress the length and width of the rectangular environment: environments with shape $2,800 \times 2,800$, $3,600 \times 3,600$, $2,800 \times 3,600$, $4,000 \times 2,400$, $2,400 \times 4,000$. In the second group, we insert random straight barriers into the environments. Note that this alters the firing fields of boundary vector cells and thus the connected place cells. These are presented as Environments 1-5 and 6-10 in Figure 3.

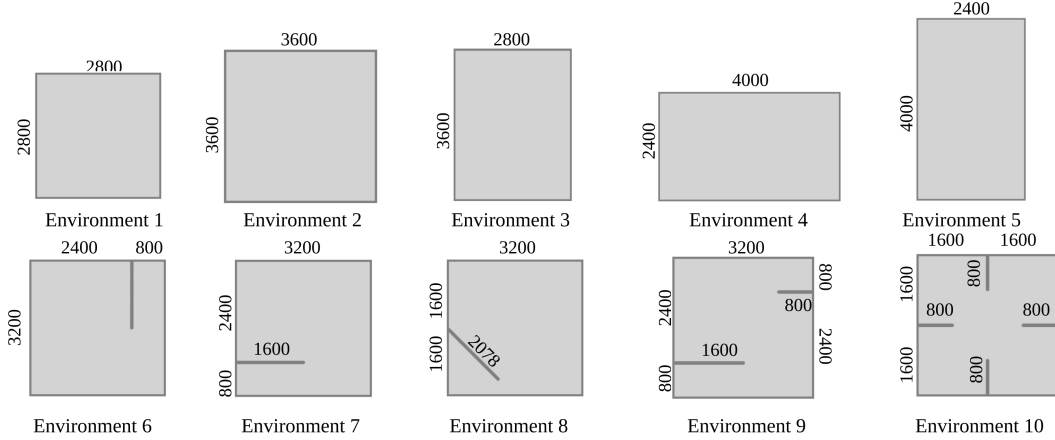


Figure 3: Diagrams showing 10 unseen environments.

In both groups, we evaluate the performance of firing field prediction using the mean squared error loss and the structural similarity index (SSIM) [28]. SSIM was designed to compare changes in quality of digital images due to compression. It has the benefit of being insensitive to shifts and translations, making it a good metric for evaluating the shape of the predicted firing fields. It is made up of three components: luminance $l(\mathbf{x}, \mathbf{y})$, contrast $c(\mathbf{x}, \mathbf{y})$ and structure $s(\mathbf{x}, \mathbf{y})$:

$$l(\mathbf{x}, \mathbf{y}) = \frac{2\mu_x\mu_y + c_1}{\mu_x^2 + \mu_y^2 + c_1} \quad c(\mathbf{x}, \mathbf{y}) = \frac{2\sigma_x\sigma_y + c_2}{\sigma_x^2 + \sigma_y^2 + c_2} \quad s(\mathbf{x}, \mathbf{y}) = \frac{\sigma_{xy} + c_3}{\sigma_x\sigma_y + c_3} \quad (10)$$

Where μ , σ , σ_{xy} are respectively the mean, bias-corrected standard deviation and bias-corrected covariance across all pixels values in \mathbf{x} and \mathbf{y} . We take $c_1 = (0.01L)^2$, $c_2 = (0.03L)^2$, and $c_3 = 0.5c_2$ where L is the maximum place cell firing rate in each firing field. The resulting SSIM is the exponentially weighted product of the three attributes from 10:

$$\text{SSIM}(\mathbf{x}, \mathbf{y}) = [l(\mathbf{x}, \mathbf{y})]^\alpha \times [c(\mathbf{x}, \mathbf{y})]^\beta \times [s(\mathbf{x}, \mathbf{y})]^\gamma \quad (11)$$

Where we consider the three attributes weighted equally: $\alpha = \beta = \gamma = 1$.

Bayesian Decoding of Agent Trajectory In this task, we test whether using the surrogate deep network, one can decode the trajectory of an agent. We consider an agent carrying the boundary vector cell–place cell neural circuit roaming freely in an unseen environment with barriers, following a Brownian motion model, inspired by the *RatInABox* package [29]. Given the recorded firing rates of boundary vector cells at each time-step, we use a Bayesian decoder to obtain a *maximum a posteriori* trajectory of the agent at each time step, comparing the decoding quality with predicted firing rates of place cells, true firing rates of place cells, predicted rate maps of place cells and true rate maps of place cells. An additional preprocessing step is required to ensure the DNN predicted firing fields and firing rates over all time steps are non-negative, thus these data needs to be pre-processed by passing through a rectifier function.

3 Results

3.1 Approximate Biological Neural Network

An initial analysis of training set output distribution (before adding Gaussian noise) by each output neurons in the ABNNs shows that the majority attains the maximum empirical entropy—the firing

rates of these neurons are different for each distinct input pattern—whereas few output neurons show unvarying outputs. This is because these neurons were assigned Sigmoidal or Tanh transfer functions so that the output is capped at 1, 0 or -1 . Further, a Principal Component Analysis [30] shows the variance of the first few eigen-directions decay slowly (2.34, 1.78, 1.41 for the first 3 principal components in the complex ABNN output). We conclude that this is an appropriate model of biological networks in the brain as a realistic model of neural circuits in the brain, as information is concentrated in a large subset of neurons, rather than a few.

Table 2: Summary of parameter search and training result with each ABNN

ABNN type	DNN	layers	units	test MSE	baseline
Feed-forward ABNN	MLP	4	256	0.1099 ± 0.0060	0.7493
Skip ABNN	MLP	3	256	0.0881 ± 0.0088	0.8530
Feed-back ABNN	MLP	2	256	0.2678 ± 0.0063	0.9991
	RNN	3	256	0.2594 ± 0.0011	
Complex ABNN	MLP	5	256	0.2472 ± 0.0052	0.7593
	RNN	8	256	0.2196 ± 0.0008	

Table 2 summarises the parameter search results, as well as the trained network performance on the test set. As a comparison, the baseline test set MSE is achieved by predicting the mean of each dimension. In all four approximate biological neural networks, the trained DNNs perform significantly better than the baseline, meaning the DNNs are able to capture some of the information processing properties of the biological counterparts. Varying the number of training data n generated from the complex ABNN, the best test set MSE loss achieved by the MLP and RNN for training up to 1,000 epochs are shown in Figure 4. Modelling plasticity changes in ABNN by injecting Gaussian noise to the connection weights, the test set loss for each value of standard deviation σ is shown in Figure 5.

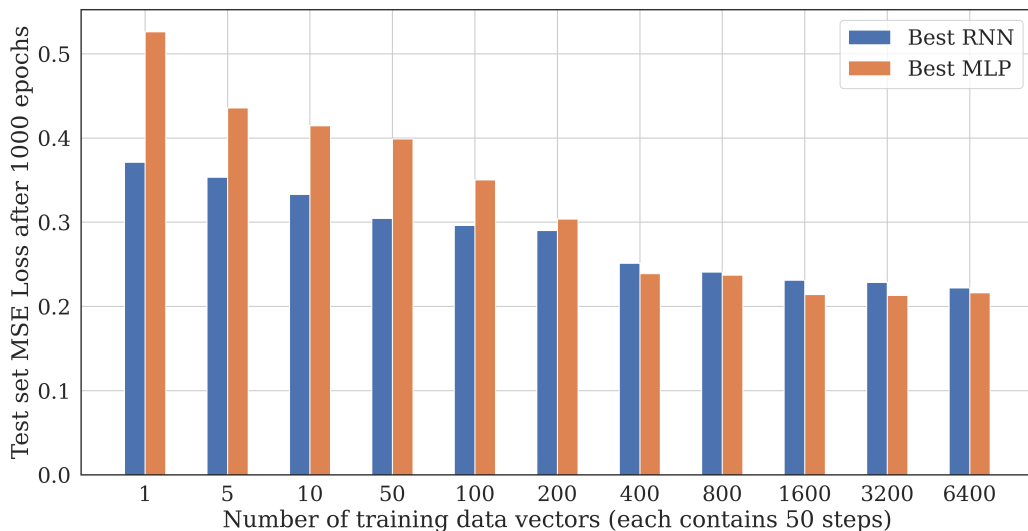


Figure 4: Best average MSE loss by each DNN achieved over 1,000 epochs, with the number of training samples specified on the X-axis.

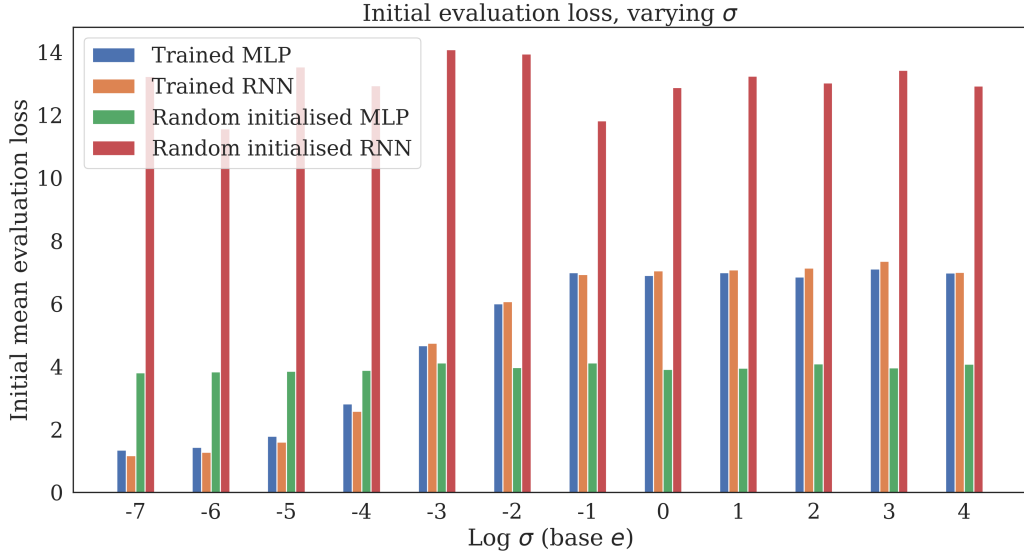
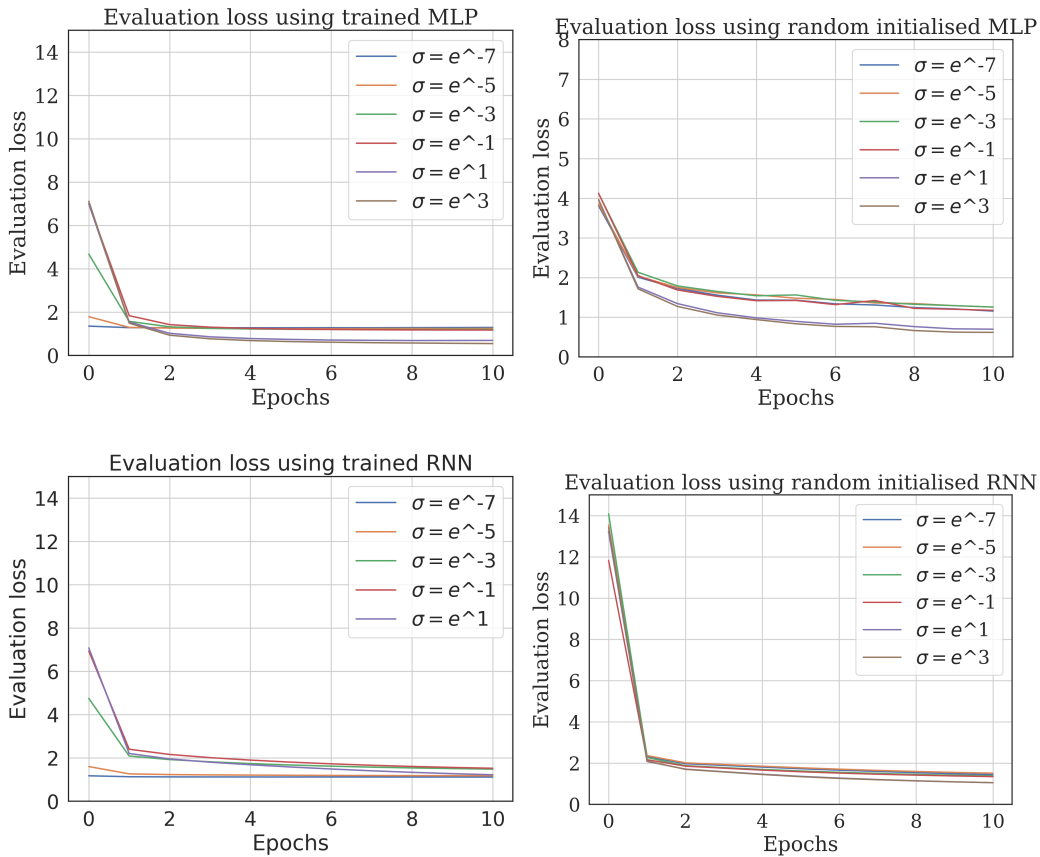


Figure 5: Average initial MSE loss (Y-axis) by: (blue) trained MLP; (orange) trained RNN; (green) a randomly initialised MLP and (red) a randomly initialised RNN over a range of noise σ (X-axis).

As a comparison, randomly initialised, untrained DNNs of the same architectures are used for the baseline test set MSE loss. The mean is taken over 30 repeats. We then proceed perform transfer learning on the trained DNNs on the new data pairs, and see if the pre-training gives any advantage compared to random initialisation. The results are shown in the figures below



3.2 Boundary Vector Cell Model

The 10 simulated place cells have the rate map as shown in Figure 2. The parameter search found a multilayer-perceptron with 6 hidden layers and 256 hidden units yields the lowest average test set MSE loss over 30 repeats. Using this network, we discretised the square environment, sampled the BVC firing rates at each mesh point and predicted the rate map of the 10 place cells. The result is shown in Figure 7, and to be compared with Figure 2.

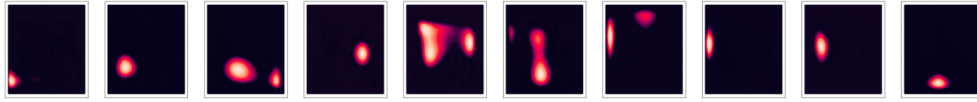
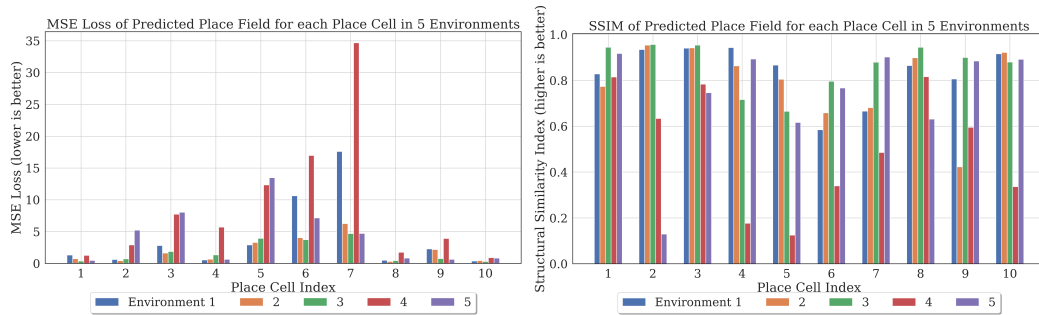


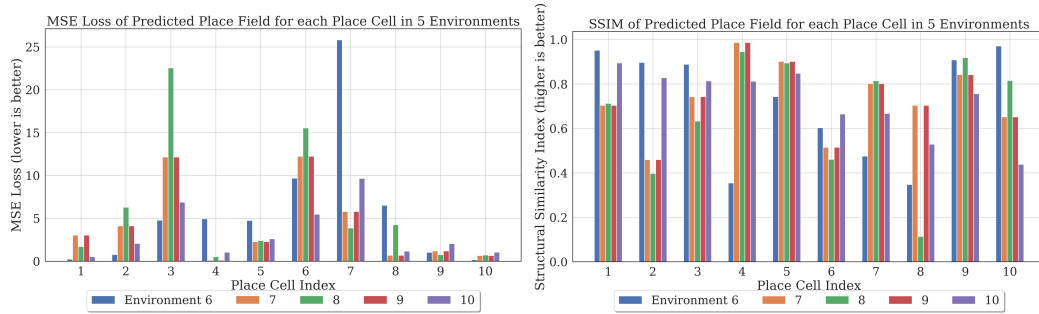
Figure 7: DNN predicted place fields of 10 simulated place cells in the environment.

The trained DNN is then tested on the 10 unseen environments created above. When evaluated using both mean squared error and SSIM. The results are illustrated in Figure 8 and Figure 9.



(a) MSE for each predicted place field for 5 environments (b) SSIM for each predicted place field for 5 environments

Figure 8: Evaluation of DNN prediction in Environments 1-5



(a) MSE for each predicted place field for 5 environments with barriers (b) SSIM for each predicted place field for 5 environments with barriers

Figure 9: Evaluation of DNN prediction in Environments 6-10

Inserting barriers into the environment changes the place fields drastically as the upstream boundary vector cells also fire in response to these barriers. Nevertheless, the trained DNN is able to predict the resulting place fields with good quality, as indicated by relatively low MSE loss (< 5) and high SSIM (> 0.6) in the majority of place cells. This shows the trained DNN was able to learn the mapping between boundary vector cell and the place cells firing rates, rather than simply remembering the place fields in the original environment. High structural similarity was also found for the majority of the place fields. An observation is that the prediction quality becomes poor when a barrier directly overlaps with the original place field, leading to a place field that disappears on one side of the barrier

(e.g. place cell 3 in Environment 7) or scatters along the end of the environment (e.g. place cell 1 in Environment 7).

A random trajectory of an agent roaming in Environment 10 is shown in Figure 10. We used a Bayesian *maximum a posteriori* rate decoder to decode the trajectory using simulated boundary vector cell firing rates and (1) DNN predicted place cell rate maps and firing rates; (2) simulated place cell rate maps and firing rates; (3) DNN predicted firing rates and simulated place cell rate maps. For three cases respectively, 88.8%, 46.6% and 1.2% of all locations were within 320 mm (10 discretised grid points by Manhattan distance) of the true location.

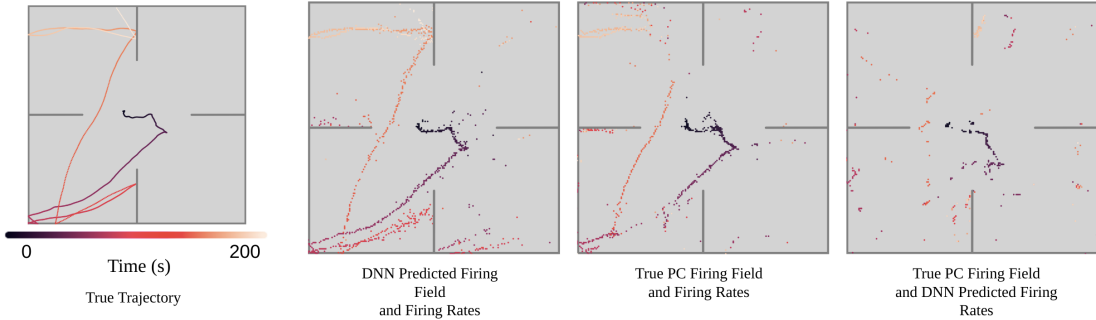


Figure 10: From left to right: true trajectory, decoded trajectories using (1) DNN predicted place cell rate maps and firing rates; (2) simulated place cell rate maps and firing rates; (3) DNN predicted firing rates and simulated place cell rate maps.

4 Discussion

Our results found that in feed-back and complex ABNNs, training with recurrent neural network with a single LSTM layer generalises better than vanilla neural networks. We believe this is because the LSTM layer is able to capture temporal dynamics due to the inclusion of feed-back and lateral inhibition connections. Furthermore, it was found that during training, MLPs converged in both training and test set MSE loss after 100 – 200 epochs and begins to over-fit shortly afterwards, whereas the LSTM losses decreasing asymptotically over the entirety of 1,000 epochs. This shows that the MLP requires less computational resources while providing a predicting power not significantly worse than the RNN. In all four ABNNs, we found DNNs with 256 hidden units and a similar number of hidden layers perform optimally, matching the ABNN counterpart.

We also see that supervised learning on the ABNN is extremely data efficient. The DNNs produced 32.2% (for RNN) and 22.9% (for MLP) higher loss when trained on only 200 out of 10,000 data samples compared to 10,000. The loss differences are reduced to 9.7% (for RNN) and insignificant (for MLP) when increasing the number of training samples to 1,600 data samples reduces the loss differences to . This result aligns with the neuroscientific observations that our brains learn with high efficiency [31], and draws correspondence between trained DNNs and real brain networks. In the generalisation and plasticity experiment, we first notice that randomly initialised RNNs yield much higher loss than any other networks, including the randomly initialised MLPs. We suspect that this is due to the weight initialisation mechanism being different in the LSTM layer—resulting in a drastically different range of predicted output upon presenting the biologically interpretable input patterns. Secondly, we observe that the performances of trained networks are better than untrained networks up to $\sigma = e^{-4.0}$, equivalent to 1.8% of the standard deviation of the originally initialised weights—it should be recognised that every synaptic connection in a neural circuit undergoes 1.8% change is quite considerable. Finally, we see that the trained DNNs at $\sigma > e^{-2.0}$ performs worse than any randomly initialised MLP. We believe that this is due to a *distributional shift* in the dataset—the weights in the ABNN underwent substantial change such that the output patterns have a completely different distribution from the original ones. The trained DNNs were fit to the original output patterns, hence producing high loss. This can be seen as performing *domain adaptation*. When retrained to fit the plasticity-altered dataset, whilst the advantage of transfer learning can be seen in small σ , we found that the performance quickly becomes indistinguishable after the

first few epochs compared to randomly initialised DNNs and the MSE loss converges to similar values.

Training the DNN using data pairs sampled from the environments using the Boundary Vector Cell model finds high prediction accuracy in the rate maps of all 10 place cells, which are visually indistinguishable. Testing the trained DNN in unseen environments (Environments 1-5) sees it generalises with relatively high accuracy in environments with similar boundary length as the environment it was trained on: shrinking or expanding the environment by $1/7$ (Environment 1 and 2) sees the majority of place cell firing fields predicted with low (< 2.0) MSE and high (> 0.6) SSIM. Changing the aspect ratio slightly (Environment 3) does not seem to affect the prediction quality by a large margin. By changing the environmental size and shape more drastically, the DNN prediction quality is further reduced (Environment 4 and 5). Nevertheless, the DNNs seems to yield good results for place cells whose firing fields are near the border of the environment (place cell indices 1 and 8).

Inserting barriers into the environment changes the place fields drastically as the upstream boundary vector cells also fire in response to these barriers. Nevertheless, the trained DNN is able to predict the resulting place fields with good quality, as indicated by relatively low MSE loss (< 5) and high SSIM (> 0.6) in the majority of place cells. This shows the trained DNN was able to learn the mapping between boundary vector cell and the place cells firing rates, rather than simply remembering the place fields in the original environment. High structural similarity was also found for the majority of the place fields. An observation is that the prediction quality becomes poor when a barrier directly overlaps with the original place field, leading to a place field that disappears on one side of the barrier (e.g. place cell 3 in Environment 7) or scatters along the end of the environment (e.g. place cell 1 in Environment 7).

Having observed a time series of boundary vector cell firing rates, one can decode the trajectory with fairly high confidence using a trained DNN with the additional pre-processing step, without needing to explicitly record the rate maps and firing rates of the downstream place cells. Of all decoded steps in three cases, it is unclear why the decoding using DNN predictions appear better than using true place cell data, but we suspect this is due to the extra pre-processing step eliminating many of the possible decoded locations. We also note that the decoding quality is restricted by many factors and cannot be fully attributed to the DNN’s performance. Firstly, the firing fields of the 10 simulated place cells do not cover the entire environment, this leads to many locations where no spikes are predicted. Secondly, the MAP estimate is a point estimate and does not convey uncertainty of the posterior distribution. Lastly, the decoding quality is restricted by the spatial resolution as a result of discretisation.

4.1 Future Works and Improvements

Our experimental approaches to approximating biological neuronal circuits, albeit simplified and preliminary, have demonstrated promising potentials in the use of modern deep learning techniques in modelling the computations and inferring the cerebral functions encapsulated in these circuits.

Various limiting factors can be identified in the ABNN that deviate from real circuits. Firstly, our input patterns are generated by counting the number of spikes at discrete time bins in simulated spike trains. The mean firing rates of each input neuron is fixed and pre-specified. This simplifying assumption can be extended by adopting dynamic firing rates for each input neuron as (possibly random) functions of an underlying, low-dimensional latent time-series of neural states driven by continuous stimuli [32]. Secondly, we interpret the output of the ABNN as the (signed) firing rates of each output neuron. In reality, information is encoded within spike timings. To this end, Spiking Neural Networks [33] could act as viable alternatives for the ABNNs and the DNNs would predict spike timings and/or intervals upon presenting inputs. Finally, in the plasticity analysis, we model the weight changes in the ABNN as injecting Gaussian noise to weights. While pragmatic, a more realistic scheme would be to present patterns to the ABNN and train it with biologically plausible learning rules, such as the BCM rule [34] or Hebb’s rule [35], or in the case of Spiking Neural Networks, with Spike Timing Dependent Plasticity [36].

Using the trained DNN for the BVC-PC network, we demonstrated that the receptive field of downstream neurons can be predicted with relatively high accuracy. However, it is non-trivial to choose a universal evaluation criterion—in our experiments we used mean squared error loss and

Structural Similarity Index. We argued that each criterion has an advantage in its own right, but is nonetheless sensitive to factors resolved by others. For example, MSE loss penalises pixel-wise differences in predicted outputs, but does it take into account translational invariance of place field over the environment. Further, we demonstrated that one can decode the predicted place cell activities to create a cognitive map of the environment. A natural step forward is to test if the trained DNN can fully replace the biological circuit to replicate behaviours in relation to spatial cognition, such as goal-directed reinforcement learning in an environment, similar to experiments conducted by Banino et al. [37].

Modern experimental neuroscience techniques have allowed precision tracing of functional neural pathways, for example, retrograde and anterograde tracing using fluorescence-labelled viruses [38]. Advancements in neuronal population recording equipment such as Neuropixel probes [39] have also pushed forward our understandings of neural information processing. While our experiments have been conducted entirely *in silico*, our ultimate goal is to use a trained DNN fully in place of a biological circuit. Having an accurate DNN as functional connectome of a brain region allows much simpler and non-invasive experimental procedures for neuroscientists, without the need to explicitly record simultaneous neuronal firings. Therefore, future work should also incorporate training the DNN on experimentally recorded firing data, and testing its robustness against stochasticity in neuronal firings, biological change in synaptic strengths, as well as cell deaths.

References

- [1] Ian Goodfellow, Yoshua Bengio and Aaron Courville. *Deep learning*. MIT press, 2016.
- [2] Jiuxiang Gu et al. “Recent advances in convolutional neural networks”. In: *Pattern recognition* 77 (2018), pp. 354–377.
- [3] Tom Young et al. “Recent trends in deep learning based natural language processing”. In: *IEEE Computational Intelligence Magazine* 13.3 (2018), pp. 55–75.
- [4] Yuxi Li. “Deep reinforcement learning: An overview”. In: *arXiv preprint arXiv:1701.07274* (2017).
- [5] David E Rumelhart, Geoffrey E Hinton and Ronald J Williams. “Learning representations by back-propagating errors”. In: *nature* 323.6088 (1986), pp. 533–536.
- [6] Kurt Hornik, Maxwell Stinchcombe and Halbert White. “Multilayer feedforward networks are universal approximators”. In: *Neural networks* 2.5 (1989), pp. 359–366.
- [7] Frank Rosenblatt. “The perceptron: a probabilistic model for information storage and organization in the brain.” In: *Psychological review* 65.6 (1958), p. 386.
- [8] Sepp Hochreiter and Jürgen Schmidhuber. “Long short-term memory”. In: *Neural computation* 9.8 (1997), pp. 1735–1780.
- [9] Caswell Barry and Neil Burgess. “Learning in a geometric model of place cell firing”. In: *Hippocampus* 17.9 (2007), pp. 786–800.
- [10] David Beniaguev, Idan Segev and Michael London. “Single cortical neurons as deep artificial neural networks”. In: *Neuron* 109.17 (2021), pp. 2727–2739.
- [11] Toviah Moldwin and Idan Segev. “Perceptron learning and classification in a modeled cortical pyramidal cell”. In: *Frontiers in computational neuroscience* 14 (2020), p. 33.
- [12] Michael L Hines and Nicholas T Carnevale. “NEURON: a tool for neuroscientists”. In: *The neuroscientist* 7.2 (2001), pp. 123–135.
- [13] Tian Wang et al. “Predicting Spike Features of Hodgkin-Huxley-Type Neurons With Simple Artificial Neural Network”. In: *Frontiers in computational neuroscience* (2022), p. 131.
- [14] Steven A Prescott, Yves De Koninck and Terrence J Sejnowski. “Biophysical basis for three distinct dynamical mechanisms of action potential initiation”. In: *PLoS computational biology* 4.10 (2008), e1000198.
- [15] A Simulation-Based Tutorial et al. “Transfer Functions in Artificial Neural Networks”. In: (2005).
- [16] Ognen AC Petroff. “Book review: GABA and glutamate in the human brain”. In: *The Neuroscientist* 8.6 (2002), pp. 562–573.
- [17] John H Byrne. “Introduction to neurons and neuronal networks”. In: *Textbook for the Neurosciences* (2013), p. 12.

- [18] Edward M Callaway. “Feedforward, feedback and inhibitory connections in primate visual cortex”. In: *Neural Networks* 17.5-6 (2004), pp. 625–632.
- [19] Daniel Jiwoong Im, Rutuja Patil and Kristin Branson. “Are skip connections necessary for biologically plausible learning rules?” In: *arXiv preprint arXiv:2001.01647* (2019).
- [20] Suzana Herculano-Houzel. “The human brain in numbers: a linearly scaled-up primate brain”. In: *Frontiers in human neuroscience* (2009), p. 31.
- [21] SW Kuffler, R Fitzhugh and HB Barlow. “Maintained activity in the cat’s retina in light and darkness”. In: *The Journal of general physiology* 40.5 (1957), pp. 683–702.
- [22] David A McCormick. “Membrane potential and action potential”. In: *From Molecules to Networks*. Elsevier, 2014, pp. 351–376.
- [23] Wei Ji Ma et al. “Bayesian inference with probabilistic population codes”. In: *Nature neuroscience* 9.11 (2006), pp. 1432–1438.
- [24] Diederik P Kingma and Jimmy Ba. “Adam: A method for stochastic optimization”. In: *arXiv preprint arXiv:1412.6980* (2014).
- [25] Colin Lever et al. “Boundary vector cells in the subiculum of the hippocampal formation”. In: *Journal of Neuroscience* 29.31 (2009), pp. 9771–9777.
- [26] John O’Keefe and Jonathan Dostrovsky. “The hippocampus as a spatial map: Preliminary evidence from unit activity in the freely-moving rat.” In: *Brain research* (1971).
- [27] Tom Hartley et al. “Modeling place fields in terms of the cortical inputs to the hippocampus”. In: *Hippocampus* 10.4 (2000), pp. 369–379.
- [28] Mykola Ponomarenko et al. “Structural similarity index with predictability of image blocks”. In: *2018 IEEE 17th International Conference on Mathematical Methods in Electromagnetic Theory (MMET)*. IEEE, 2018, pp. 115–118.
- [29] Tom M George et al. “RatInABox: A toolkit for modelling locomotion and neuronal activity in continuous environments”. In: *bioRxiv* (2022).
- [30] Karl Pearson. “LIII. On lines and planes of closest fit to systems of points in space”. In: *The London, Edinburgh, and Dublin philosophical magazine and journal of science* 2.11 (1901), pp. 559–572.
- [31] Martijn P Van Den Heuvel et al. “Efficiency of functional brain networks and intellectual performance”. In: *Journal of Neuroscience* 29.23 (2009), pp. 7619–7624.
- [32] Byron M Yu et al. “Gaussian-process factor analysis for low-dimensional single-trial analysis of neural population activity”. In: *Advances in neural information processing systems* 21 (2008).
- [33] Wolfgang Maass. “Networks of spiking neurons: the third generation of neural network models”. In: *Neural networks* 10.9 (1997), pp. 1659–1671.
- [34] Elie L Bienenstock, Leon N Cooper and Paul W Munro. “Theory for the development of neuron selectivity: orientation specificity and binocular interaction in visual cortex”. In: *Journal of Neuroscience* 2.1 (1982), pp. 32–48.
- [35] Donald Olding Hebb. *The organization of behavior: A neuropsychological theory*. Psychology Press, 2005.
- [36] Biswadeep Chakraborty and Saibal Mukhopadhyay. “Characterization of Generalizability of Spike Timing Dependent Plasticity Trained Spiking Neural Networks”. In: *Frontiers in Neuroscience* 15 (2021), p. 695357.
- [37] Andrea Banino et al. “Vector-based navigation using grid-like representations in artificial agents”. In: *Nature* 557.7705 (2018), pp. 429–433.
- [38] Christine Saleeba et al. “A student’s guide to neural circuit tracing”. In: *Frontiers in neuroscience* (2019), p. 897.
- [39] Nicholas A Steinmetz et al. “Neuropixels 2.0: A miniaturized high-density probe for stable, long-term brain recordings”. In: *Science* 372.6539 (2021), eabf4588.